Origin of the resonant x-ray scattering in LaMnO3

Gloria Subías, Javier Herrero-Martín, Joaquín García, Javier Blasco, Claudio Mazzoli, Keisuke Hatada, Sergio Di Matteo, Calogero R. Natoli

Origin of the resonant x-ray scattering in $LaMnO_3$

G. Subías,[1] J. Herrero-Martín,[1] J. García,[1] J. Blasco,[1] C. Mazzoli,[2] K. Hatada,[1,3] S. Di Matteo,[3] and C. R. Natoli[3]
[1]*Instituto de Ciencia de Materiales de Aragón (ICMA), CSIC-Universidad de Zaragoza, C\Pedro Cerbuna 12, 50009-Zaragoza, Spain*
[2]*European Synchrotron Radiation Facility, Boîte Postal 220, F-38043 Grenoble Cedex, France*
[3]*Laboratori Nazionali di Frascati INFN, via E. Fermi 40, Cassella Postale 13, I-00044 Frascati Roma, Italy*
(Received 25 January 2007; revised manuscript received 28 March 2007; published 1 June 2007)

We have performed a detailed resonant x-ray scattering (RXS) study at the Mn *K* edge of $LaMnO_3$ by measuring the $(h,0,0)$, $(0,k,0)$ and $(0,0,l)$ forbidden reflections $(h,k,l=3,5)$ between 10 and 300 K in the σ-π channel. For all three types of reflections we observed strong resonant peaks presenting the $\sin^2\phi$ intensity modulation as a function of the azimuth scanning angle ϕ, characteristic of dipolar transitions. Their origin was ascribed to anisotropic tensor scattering, since no change either in energy line shape or in intensity was observed when crossing the Néel temperature at ~140 K. Integrated intensities were roughly constant up to 300 K, contrary to previous reports found in the literature. The energy dependence of the scattered intensity for the $(h,0,0)$ and $(0,k,0)$ reflections was identical but different from the $(0,0,l)$ reflection. All reflections have been explained within multiple scattering theory in terms of long-range structural distortions around Mn atoms, without invoking any kind of 3*d* orbital ordering. We also studied the energy dependence of the principal axes of the anomalous-scattering tensor in a case, like the present one, where the scattering atoms do not possess any point-symmetry axes. We found that they are not constant with the photon energy, implying the absence of a direct correlation between RXS and quadrupolar charge distribution in the ground state.

DOI: 10.1103/PhysRevB.75.235101 PACS number(s): 75.47.Lx, 78.70.Ck, 75.50.Ee, 61.10.−i

I. INTRODUCTION

Orbital physics in transition-metal oxides has been attracting great interest in the past ten years,[1,2] after it was recognized that orbital degrees of freedom (ODF) play an important role in their transport and magnetic properties, through strong coupling with charge, spin, and lattice dynamics. Among the variety of phenomena induced by the ODF, many papers focused on the possible detection of the so-called orbital ordering (OO) and its correlation with magnetic order.[3] $LaMnO_3$, which is the parent compound of the colossal magnetoresistive manganites, is the archetypical system with a *d*-OO ground state.[4] In this compound, the ODF are represented by the singly occupied doubly degenerate e_g states of the Mn^{3+}, arising from the octahedral ligand field and the strong Hund's coupling. This orbital degeneracy leads Mn^{3+} to be an active Jahn-Teller ion, i.e., the degeneracy is lifted by a nearly tetragonal distortion of the oxygen octahedron that surrounds the Mn ion.

Resonant x-ray scattering (RXS) is a powerful experimental technique to analyze structural and electronic long-range ordered phases, as the resonant signal probes the local electronic levels coherently throughout the whole crystal. Recently, the observation of resonance in the scattered intensity of the (3,0,0) forbidden reflection at Mn *K* edge in $LaMnO_3$ (Ref. 5) was initially interpreted as a direct probe of the OO: the idea behind this interpretation was that the observed splitting of Mn 4*p* levels was due to the Mn 3*d* OO through the on-site 3*d*-4*p* Coulomb interaction.[6] However, the original idea that OO could be directly probed by this technique turned out to be incorrect, for reasons outlined below and better detailed in the literature.[7–10] Briefly, detailed numerical calculations with different theoretical approaches[8,9] had shown that the observed splitting of Mn 4*p* levels was by far due to the structural distortion and just a negligible contribution came from OO. Yet, one experimental fact was left unexplained by such interpretation, i.e., the reported variation in the temperature dependence of the (3,0,0) peak above T_N.[5] The measured scattering intensity increases with decreasing temperature as the Néel temperature is approached. Supporters of the OO scenario interpreted this variation as a proof that magnetic order has a direct consequence on OO.[6]

In the present work, we report on some unresolved or unexplored issues of the experimental and theoretical aspects of RXS in $LaMnO_3$. $LaMnO_3$ is a paramagnetic insulator with orthorhombic perovskite structure (space group[11] *Pbnm*) at room temperature. In this structure, Mn ions are characterized by a local inversion symmetry and by three different bond distances with surrounding oxygen atoms: long (l~2.14 Å), intermediate (i~1.97 Å), and short (s ~1.91 Å). The long Mn-O bonds lie almost in the *ab* plane in a checkerboard type of arrangement so that $l-s-l-s$ bonds are met as one moves from Mn to Mn along the Mn-O-Mn path. This arrangement is stacked ferro-orbitally along the *c* axis. At T_{JT}=750 K, $LaMnO_3$ undergoes a structural phase transition, which has been interpreted as an order-disorder transition above which the crystallographic orthorhombic distortion disappears.[12,13] This transition is accompanied by an abrupt change in the electrical resistivity, thermoelectric power, and Weiss constant.[14] Below T_{JT}, a cooperative Jahn-Teller effect sets in, which in turn induces the OO of the e_g states. A-type antiferromagnetism (AFM) appears below T_N=140 K, in which magnetic moments on Mn sites are aligned ferromagnetically in the *ab* plane and are stacked antiferromagnetically along the *c* axis. Such a magnetic pattern was explained as arising from the OO.[15,16]

First of all, we have studied the azimuth angle and energy dependences of the (300) scattered intensity from 10 K up to room temperature, finding no variation in the integrated signal in the whole temperature range, in contrast with the results reported in Ref. 5. It is worthwhile to note that this result, if confirmed, would support the "structural" interpre-

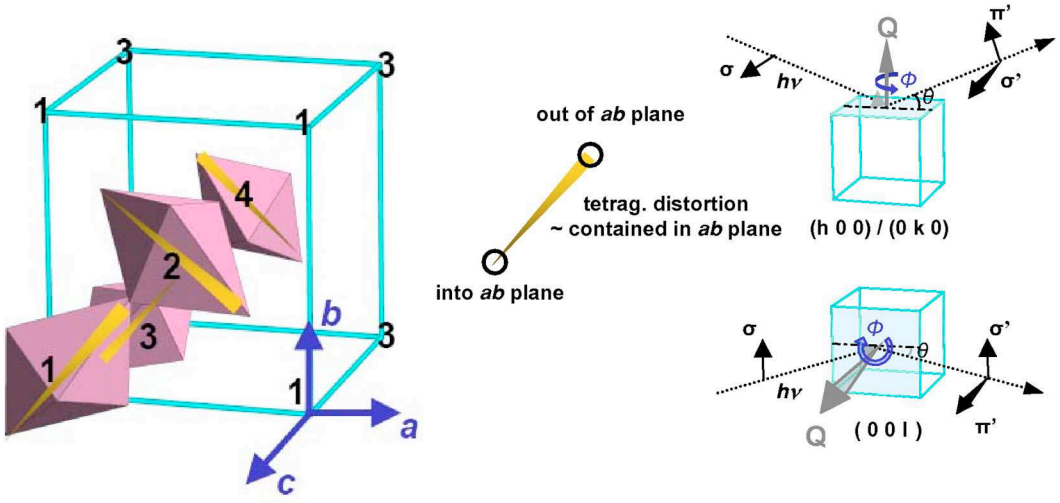

FIG. 1. (Color online) Schematic picture of the four Mn atoms in the *Pbnm* crystal cell of $LaMnO_3$ indicating the ordering of the long Mn-O bond (l). The scattering geometry and definition for polarization directions of the incident (σ) and scattered (σ', π') beams for $(h,0,0)$, $(0,k,0)$, and $(0,0,l)$ forbidden reflections are shown on the right.

tation as the only correct one and positively reject the OO interpretation. In addition to the well-known resonant forbidden reflections such as (3,0,0), (5,0,0), (0,3,0), and (0,5,0), we have also measured the (0,0,3) and (0,0,5) reflections, related to the A-antiferromagnetic propagating vector. Differently from neutron scattering,[17] however, the observation of a RXS signal for the $(0,0,2n+1)$ reflections is shown to be a signature of the (threefold) anisotropy of the Mn p band (see Sec. IV). We demonstrate that the RXS signal at these $(0,0,2n+1)$ reflections has a different origin than the one at $(2n+1,0,0)$ reflections, as a bigger cluster than a simple MnO_6 distorted octahedron must be considered in order to correctly describe them theoretically. We also identify as a general feature of RXS the dependence on energy of the principal axes of the electric quadrupole tensor in the excited states when no local symmetry axes are present at the site of the resonating atom. Finally, we show experimentally that the magnetic ordering has no influence in any of the observed RXS signals. The analysis of the energy, azimuth, and polarization dependences of the RXS signals was performed by calculating the tensorial components of the anomalous atomic scattering factor through two codes in the multiple scattering mode: MXAN (Ref. 18) and FDMNES.[19]

II. EXPERIMENTAL DETAILS

Single crystals of $LaMnO_3$ were grown at our own laboratory (ICMA, Zaragoza) using a halogen lamp floating zone furnace. The crystals were characterized by means of x-ray powder diffraction and ac magnetic susceptibility. The crystal structure was *Pbnm* (a=5.531 Å, b=5.740 Å, and c=7.688 Å at 300 K) and the oxygen stoichiometry $LaMnO_{2.99\pm0.01}$ was determined by redox titration analysis. The magnetic measurements showed an antiferromagnetic transition at $T_N \sim 140$ K as reported for stoichiometric $LaMnO_3$.[11] Two crystals were cut and polished to either (100)/(010) or (001) flat surfaces. We note that [100] and [010] domains occur at the same surface because of twinning. However, the relatively strong orthorhombic distortion makes the $(h,0,0)$ and $(0,k,0)$ reflections occur at different scattering angles so they can be separately studied.

RXS experiments have been performed at the ID20 beamline[20] of the European Synchrotron Radiation Facility (ESRF) in Grenoble, France. The incident beam was monochromatized by a double crystal Si(111) that delivers a 99% linearly polarized beam, with polarization perpendicular to the scattering plane (σ). The typical energy resolution is 0.7 eV at the Mn K edge. Single crystals were mounted inside a closed-cycle helium refrigerator, allowing us to measure the temperature dependence of the studied reflections from 10 K up to room temperature, with the vector normal to the surface lying in the scattering plane. This in turn was mounted within the four-circle vertical diffractometer. A scheme of the crystallographic unit cell together with the scattering geometry is shown in Fig. 1. Azimuthal scans were measured by rotating the sample around the scattering vector (**Q**). A Cu(220) crystal positioned between the sample and the detector has been used to analyze whether the polarization of the scattered beam is parallel (π') or perpendicular (σ') to the vertical scattering plane.

III. RESULTS

Figure 2 shows the energy dependence of the six forbidden reflections $(h,0,0)$, $(0,k,0)$, and $(0,0,l)$ [h, k, l=3 or 5] at T=10 K for the σ-π' polarization channel. The fluorescence spectrum is also shown as an energy reference. A strong enhancement of the σ-π' intensity in all reflections has been observed only at energies close to the Mn K absorption edge. No intensity was observed for the σ-σ' polarization channel at any of the studied reflections. Moreover, the resonant intensity is independent of the scattering vector, which implies that only dipole-dipole transitions contribute. The $(h,0,0)$ and $(0,k,0)$ reflections, in particular, have iden-

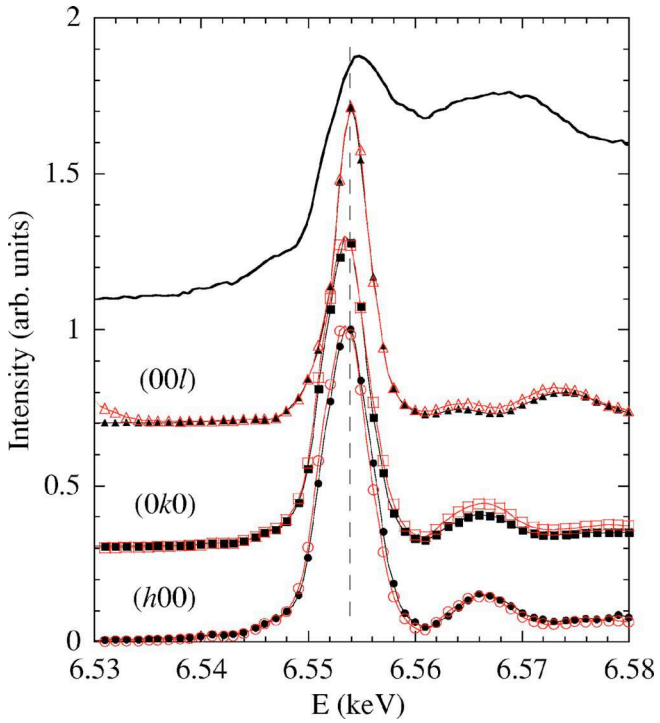

FIG. 2. (Color online) Energy dependence of the forbidden (3,0,0), (0,3,0), and (0,0,3) (solid black symbols) reflections compared with the (5,0,0), (0,5,0), and (0,0,5) (open red symbols) ones in the σ-π' channel near the Mn K edge at the azimuth angle $\phi=0°$, together with the fluorescence spectrum (upper curve). Intensities are scaled to the maximum and shifted along the y axis for comparison.

tical energy dependence: this is consistent with the fact that the structure factors for these two reflections are the same, as shown in Sec. IV. On the other hand, the resonance observed at the forbidden $(00l)$ reflections is different from that reported for either the $(h,0,0)$ or the $(0,k,0)$ ones, as its maximum and its rising edge are slightly shifted to higher energies and the intensity is lower. This is a clear indication that the resonant signal at the $(0,0,l)$ reflections has a different origin. We note here that $(0,0,2n+1)$ reflections correspond to the periodicity of the antiferromagnetic ordering of $LaMnO_3$. However, the observed resonant scattering cannot arise from the magnetic order as these reflections also appear in the paramagnetic phase at room temperature. Their structural origin is demonstrated theoretically in the next section.

When the crystal is rotated around the scattering vector, the σ-π' intensity of the three types of reflections exhibits a characteristic $\sin^2\phi$ dependence, ϕ being the azimuth angle. The inset in Fig. 3 compares the azimuth dependence of the integrated intensity at the (3,0,0), (0,3,0), and (0,0,3) reflections, measured by sample rocking curves (θ scans) at the same energy (6554 eV) and normalized by the respective fundamental (4,0,0), (0,4,0), and (0,0,4) reflections. The maximum intensity corresponds to the incident polarization vector parallel to [010], [100], and [010] directions for $(h,0,0)$ $(0,k,0)$, and $(0,0,l)$ reflections [h, k, l=3 or 5], respectively. The energy line shape of the resonance does not change by varying the azimuth angle, except for a scale factor, as it is shown for the (0,0,5) reflection in Fig. 3. We note that our results concur with those obtained previously at the (3,0,0) forbidden reflection.[5,21]

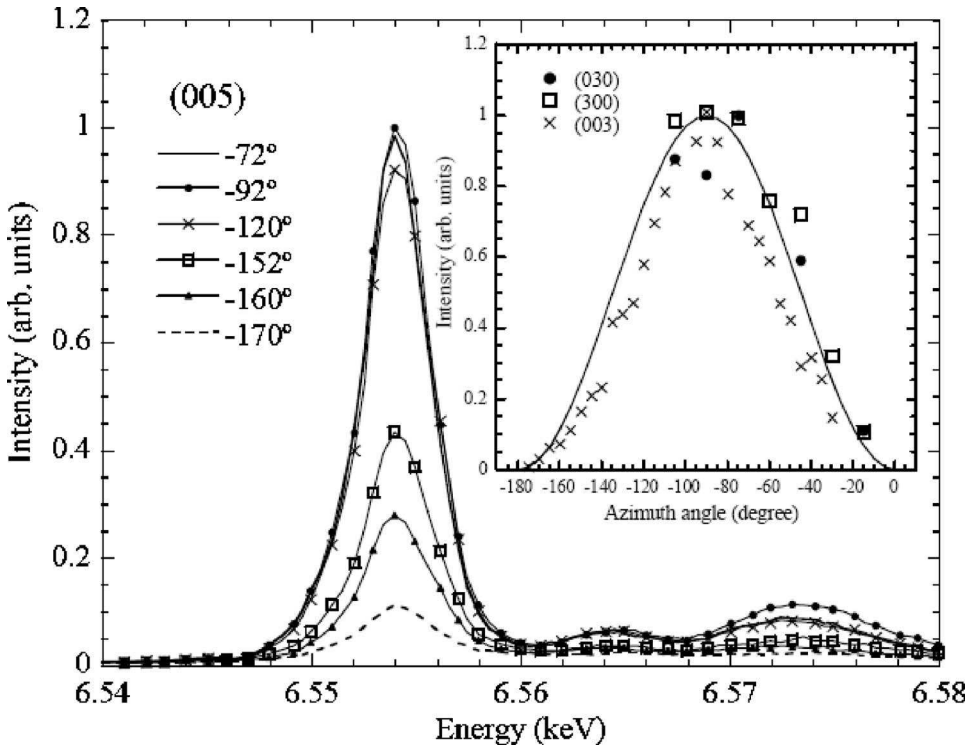

FIG. 3. Energy dependence of the forbidden (0,0,5) reflection measured at different azimuth angles. Inset: The azimuthal angular dependence of the integrated intensity at $E=6554$ eV, which corresponds to the maximum resonance intensity for the three types of forbidden reflections. The solid curve is the calculated intensity of Eq. (4).

With the aim of determining whether any correlation exists between the observed RXS and the magnetic ordering, we have also measured the temperature dependence of the σ-π' integrated intensities at resonance for each of the six reflections. Figure 4 plots the temperature dependence of the resonant scattering at the six reflections between 10 and 300 K. The resonant intensities are approximately constant for the whole temperature range within the experimental error. It is noteworthy that these results are in contrast with those reported by Murakami *et al.*,[5] who observed a decrease of the resonant intensity of the (3,0,0) reflection above the Néel temperature. The absence of any intensity variation around T_N is important because such a variation represented the unique unexplained feature in the generally accepted interpretation of the (300) RXS at Mn *K* edge[8,9] in terms of structural distortion. Therefore, our results indicate that there is no correlation between the resonant scattering and the long-range AFM ordering and they absolutely discard any kind of role for an OO in the RXS at the Mn *K* edge. Moreover, the results for the $(0,0,2n+1)$ reflections are particularly relevant, since these reflections are clear signatures of the AFM ordering in neutron-scattering patterns.[17] We checked that identical energy and azimuth dependence of the scattered intensity were observed at two selected temperatures, one above and the other below T_N. This confirms that all signals are entirely due to (non-magnetic) Templeton scattering in the whole temperature range.

IV. THEORETICAL FRAMEWORK

Core resonant spectroscopies are described by the virtual processes that promote a core electron to some empty energy levels. In particular, RXS is originated by the virtual absorption of a photon of energy $\hbar\omega = E_b - E_a$, determining the electron transition from a ground state $|a\rangle$, with energy E_a, to an intermediate excited state $|b\rangle$, with energy E_b, followed by a successive relaxation process and the emission of a photon with the same energy $\hbar\omega$. This process is coherent throughout the crystal, giving rise to the usual Bragg diffraction condition. The resonant scattering probability amplitude in the dipole approximation is proportional to[22]

$$f \propto \sum_b \frac{\langle a|(e' \cdot r)|b\rangle\langle b|e \cdot r|a\rangle}{E_a + \hbar\omega - E_b - i\Gamma_b/2}, \tag{1}$$

where the term $i\Gamma_b/2$ takes into account the lifetime of the intermediate state $|b\rangle$, and e and e' are the incoming and outgoing x-ray polarizations.

The dipole approximation is fully justified at the *K* edge of transition-metal oxides, provided pre-edge features are absent as in the present case. Far from the absorption edge, resonant scattering is negligible. At forbidden reflections, the Thomson term is identically zero and only Eq. (1) contributes to the scattering amplitude. In this case, we can expand the scalar products in Eq. (1) in order to factorize the total atomic scattering factor (ASF) as $f(\mathbf{e},\mathbf{e}') = e_m e'_n f^{mn}$. The second-rank symmetric tensor f^{mn} only describes the sample properties and is independent of radiation. For octahedral and tetrahedral symmetries of the resonating atom, the f^{mn} tensor is diagonal and all three components are equal to each other, so that the tensor behaves as a scalar. For all the remaining symmetries, the tensor components are different and the scattering power depends on the relative orientation of the local geometrical structure around the (absorbing) scattering atom and the electric polarization vectors.[23,24] The tensor character of the ASF measures the anisotropy of the empty electronic levels of the resonating atom. In particular, the second-rank, traceless, symmetric tensor f^{mn} is proportional to the electric quadrupole expectation value in the excited $|b\rangle$ states at the energy E_b.[25] As any symmetric tensor can be reduced in a diagonal form in a proper reference frame (principal axes), it is worthwhile to investigate whether it is possible to find out the principal directions of the electric quadrupole ellipsoid and if these directions are constant in energy or not.

The ASF tensor in the crystallographic frame with x, y, and z along a, b, and c crystal axes (Fig. 1) can be described generically as

$$f_{\mathrm{Mn}} = \begin{pmatrix} f_{xx} & f_{xy} & f_{xz} \\ f_{xy} & f_{yy} & f_{yz} \\ f_{xz} & f_{yz} & f_{zz} \end{pmatrix}. \tag{2}$$

In the unit cell of $LaMnO_3$, there are four Mn^{3+} atoms at equivalent positions (*Pbnm* setting): $Mn_1 = (0,0,0)$, Mn_2

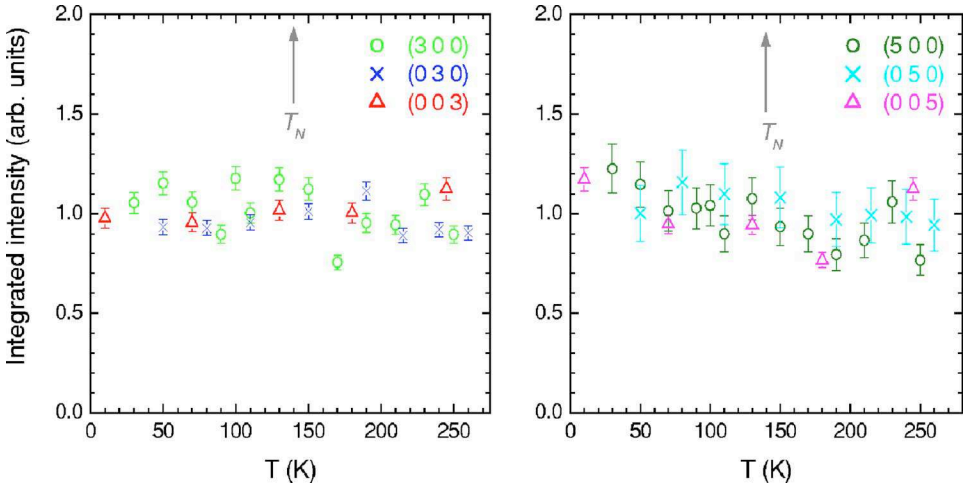

FIG. 4. (Color online) Temperature dependence of the integrated intensity of the $(h,0,0)$, $(0,k,0)$, and $(0,0,l)$, with h, k, l =3 or 5 reflections on resonance, normalized for comparison.

$=(1/2,1/2,0)$, $Mn_3=(0,0,1/2)$, and $Mn_4=(1/2,1/2,1/2)$. The structure factor at both $(2n+1,0,0)$ and $(0,2n+1,0)$ reflections is $F_{(odd,0,0)}=F_{(0,odd,0)}=f_{Mn1}+f_{Mn3}-f_{Mn2}-f_{Mn4}$, while the structure factor at $(0,0,2n+1)$ is $F_{(0,0,odd)}=f_{Mn1}+f_{Mn2}-f_{Mn3}-f_{Mn4}$. The four sites are related by the following symmetry operations: $Mn_2=\hat{m}_aMn_1$, $Mn_3=\hat{m}_cMn_1$, and $Mn_4=\hat{m}_bMn_1$, where $\hat{m}_a$, $\hat{m}_b$, and $\hat{m}_c$ are the mirror planes orthogonal to the crystal axes a, b, and c. Therefore, $F_{(odd,0,0)}=(1+\hat{m}_c-\hat{m}_a-\hat{m}_b)f_{Mn1}$ and $F_{(0,0,odd)}=(1+\hat{m}_a-\hat{m}_c-\hat{m}_b)f_{Mn1}$. Remembering that $\hat{m}_a(x,y,z)=(-x,y,z)$, $\hat{m}_b(x,y,z)=(x,-y,z)$, and $\hat{m}_c(x,y,z)=(x,y,-z)$, the structure factor tensors are then reduced to

$$F_{(odd,0,0)}=F_{(0,odd,0)}=4\begin{pmatrix}0 & f_{xy} & 0\\ f_{xy} & 0 & 0\\ 0 & 0 & 0\end{pmatrix}$$

and

$$F_{(0,0,odd)}=4\begin{pmatrix}0 & 0 & 0\\ 0 & 0 & f_{yz}\\ 0 & f_{yz} & 0\end{pmatrix}. \quad (3)$$

We can deduce from this analysis that $(0,0,2n+1)$ reflections give information on different off-diagonal components of the ASF tensor compared to the $(2n+1,0,0)$ and $(0,2n+1,0)$ reflections.

Finally, the intensities corresponding to the above structure factors in the σ-σ' polarization channel are equal to zero, while in the σ-π' polarization channel the intensities are given by

$$I(2n+1,0,0)=I(0,2n+1,0)=16f_{xy}^2\cos^2\theta\sin^2\phi,$$

$$I(0,0,2n+1)=16f_{yz}^2\cos^2\theta\sin^2\phi. \quad (4)$$

Here, θ is the Bragg angle and ϕ is the azimuth angle as defined in Fig. 1. For the two types of reflections, only the σ-π' polarization channel is active and the azimuth dependence is of a $\sin^2\phi$ type as was experimentally measured. We observe that the azimuth and polarization dependences are only determined by crystallography and the unique condition for these forbidden reflections to be observed is that f_{xy} and f_{yz} should be different from zero.

In order to describe the energy dependence of the RXS spectra, we have calculated the ASF tensor in the multiple-scattering approach. Both FDMNES and MXAN codes were used to calculate the different terms of the ASF tensor (real and imaginary parts). The calculation was performed for a cluster radius of 5.75 Å, i.e., 63 atoms. We used the atomic coordinates determined by crystal studies.[11] The two codes gave equivalent results. Figure 5 shows the comparison between the experimental data of forbidden (0,3,0) and (0,0,3) reflections with the calculated $|f_{xy}|^2$ and $|f_{yz}|^2$ terms, respectively, obtained with the MXAN program. The agreement with experience is quite good, as the rising edge of the (0,3,0) and (3,0,0) reflections are lower in energy than that of the (0,0,3) reflection, whereas the falling edges of all three are at the same energy, as found experimentally.

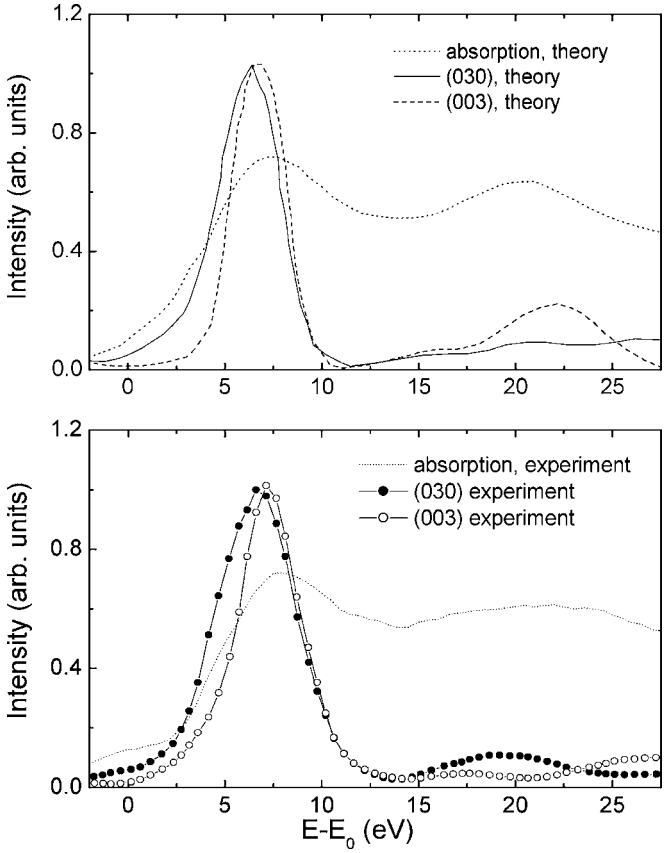

FIG. 5. Calculated RXS of the (030) and (003) forbidden reflections together with the absorption spectrum. Upper panel, calculation with the MXAN code using a cluster of 63 atoms. Lower panel, experimental data. The spectra are scaled to the maximum.

We can compare these results with the calculation of the ASF tensor using a smaller cluster radius of 3 Å, i.e., just including the first oxygen coordination shell. The results are displayed in Fig. 6, and we observe that within this simpler MnO_6 cluster, the three forbidden reflections are still present, but the agreement with the experimental data is rather qualitative, as the shift to higher energies of the maximum in the $(0,0,2n+1)$ reflections disappears and, above all, the rising

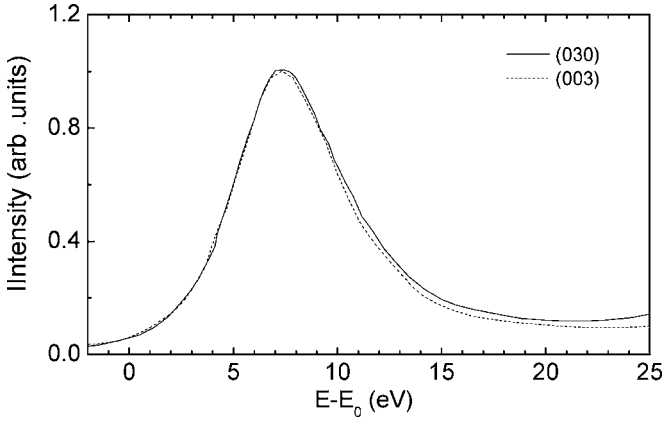

FIG. 6. Calculated RXS of the (030) and (003) forbidden reflections with the MXAN code using the MnO_6 cluster.

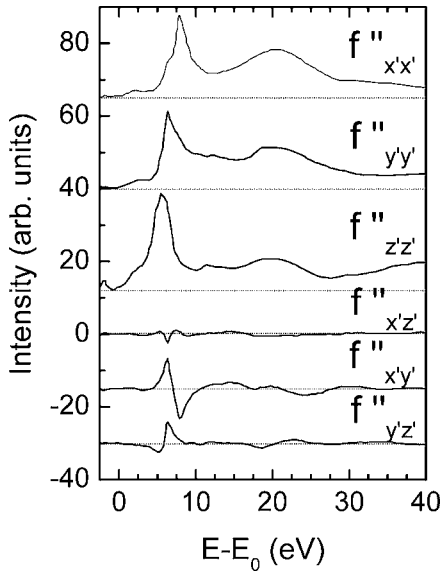

FIG. 7. Components of the ASF tensor in an orthogonal frame close to the Mn-O bond frame. Z', X', and Y' axes are nearly along the long (l), intermediate (i), and short (s) Mn-O bond directions, respectively.

edges are all at the same energy. This is a clear indication that most of the RXS signal comes from second and third nearest neighbors for the (003) reflection and, accordingly, a simple MnO_6-cluster calculation is not sufficient. We proved in this way that the physical origin of the (003) reflection is mainly related to contributions to the anisotropic form factor coming from atoms beyond the first coordination shell of the oxygen atoms. This fact is in contrast with what happens at the (300) and (030) reflections, which probe a more localized anisotropy, and is at the basis of the energy difference in the rising edges of the three reflections.

Finally, we have also investigated the behavior of the electric quadrupole moment of the Mn excited states. For this purpose, we have calculated the ASF tensor for the cluster of 63 atoms in a frame where the orthogonal axes, x', y', and z' are close to Mn-O bonds. In particular, the z' axis is along the Mn-O longer bond direction, the x' axis is approximately along the Mn-O intermediate bond, and y' is approximately along the shorter Mn-O bond. It should be remembered that the three Mn-O bonds are not exactly orthogonal due to the local distortion and, therefore, the orthogonal frame is only approximately directed along the Mn-O bonds. The new tensor coincides with the tensor in the crystallographic frame after rotation, which guarantees the consistency of our calculation. We found out that this tensor is not diagonal at all energies, as shown in Fig. 7, where all elements are drawn. This implies that the basis where the tensor is diagonal, i.e., the principal axes of the ellipsoid representing the quadrupole, changes direction at different energies. This clearly demonstrates that such a measurement is not directly related to the ground-state electric quadrupole, which, of course, has a unique direction of the principal axes. Figure 8 plots the projections of two of the three principal axes in the $x'y'$ plane and in the $y'z'$ plane. We observed that one of the eigenvector moves close to the direction of the

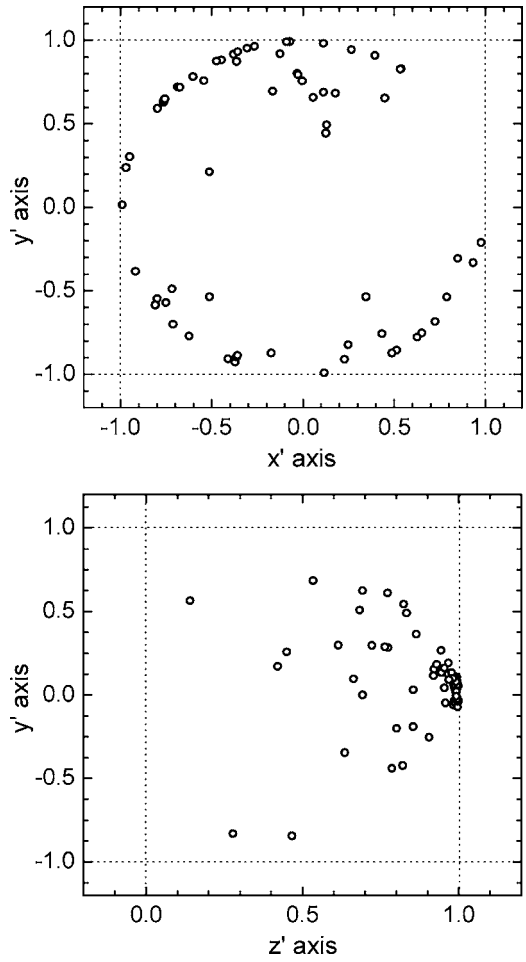

FIG. 8. Upper panel: Projection of the $V_{y'}$ eigenvector in the $x'y'$ plane. We observe that the vector is randomly distributed in the $x'y'$ circle of radius=1. Lower panel: Projection of $V_{z'}$ eigenvector in the $y'z'$ plane. The anisotropy is mainly oriented along the Mn-O longer bond.

long Mn-O bond. On the other hand, the other two eigenvectors along the principal x' and y' axes ($V_{x'}$ and $V_{y'}$) are randomly distributed in the plane determined by the short and intermediate Mn-O bonds.

This result may appear surprising if the sum rules by Carra *et al.*[26] are applied naively: these sum rules relate the excited-state measurements to the ground-state properties, but they are only valid provided the energy spread of the excited states is much less than their inverse lifetime $\Gamma_b/2$, a condition which may be fulfilled for f states of rare earths, but which is not verified for all K edges of transition-metal oxides, where $\Gamma_b/2 \approx 2$ eV and the energy spreading of the resonance is about 10 eV. In the case of K edges of transition-metal oxides, the symmetric RXS tensor f^{mn} measures the density of empty p states projected at the Mn atom as a function of their kinetic energy.[25] Thus, in the absence of any constraints like an n-fold symmetry axis, there is no physical reason forcing the quadrupole principal axes to point in the same directions at all energies. They could change direction at some energy, as has been proven in the present work.

V. DISCUSSION AND CONCLUSIONS

In the present paper we have revisited some physical consequences of Mn *K*-edge RXS in $LaMnO_3$ both experimentally and theoretically. Several conclusions can be deduced that have strong implications on the physics of $LaMnO_3$ and on the general interpretation of RXS experiments in other related transition-metal oxides.

First, as has been extensively discussed in the literature,[7–9] the RXS signal at the Mn *K* edge is just a consequence of the local distortion around the resonating atom. For example, in the case of the (3,0,0) forbidden reflection in $LaMnO_3$, the anisotropic energy shift in the *p* density of states determined by the underlying OO through the Coulomb $3d$-$4p$ repulsion is found to be negligible when compared to the equivalent shift determined by the structural distortion. However, the strong intensity variation around T_N experimentally found in Ref. 5 could never be explained through the temperature dependence of the lattice and a critique in this direction was moved by those who still believed that the forbidden (3,0,0) reflection is a signature of OO.[6] In our work, we could not find any intensity variation around T_N, consistent with the "structural" interpretation. Although further measurements in this way may be desirable, we therefore conclude that the OO interpretation of Mn *K*-edge resonant reflections is definitively untenable.

The second result of our paper is the observation of two independent forbidden reflections, which imply that in the rank-2 ASF tensor two different nonzero off-diagonal elements are needed to describe the scattering completely. The origin of the two independent reflections, (3,0,0) [or, equivalently, (0,3,0)] on one side and (0,0,3) on the other, is clearly different, as a MnO_6 cluster is sufficient in order to reproduce correctly the RXS signals at the (3,0,0) [or (0,3,0)] reflection, whereas a bigger cluster is required for the (0,0,3) reflection. Therefore, when moving along the *c* axis, the description of the ordered *p*-empty states must also include atoms beyond the first oxygen neighbors (up to 63 atoms in order to obtain a good convergence of the calculation), while the simpler description in terms of a local MnO_6 cluster is sufficient in the *ab* plane.

The third conclusion of the present paper goes beyond the physics of $LaMnO_3$ and concerns the general interpretation of anisotropic resonant scattering at transition-metal *K* edges. It deals with the fact that the principal axes of the anisotropic ASF tensor for scattering atoms with no point-symmetry elements, as occurs in $LaMnO_3$, are not constant with the photon energy. From the general point of view, this means that it is not possible to infer the direction of the principal axes of the ground-state electric quadrupole from a *K*-edge measurement and that only indirect information can be inferred. However, if the point-symmetry group of the atom site has an *n*-fold symmetry axis, this imposes a constraint on the directions of the quadrupole principal axes for all excited states, which are independent of energy. As an example, for tetragonal or trigonal distortions of the octahedron, the main axes of the anisotropic ASF tensor are aligned along the tetragonal or trigonal axis and perpendicular to it in the whole energy range.[27] Moreover, in the particular case of $LaMnO_3$ and other manganites, the approximation that the principal axes have fixed directions along the ligands can be rather good to describe some experimental results.[28] Even in the present case, the assignment of the anisotropy axes to be fixed along the long Mn-O bond in the whole energy range allows one to nicely reproduce the RXS spectra of the $(2n+1,0,0)$ and $(0,2n+1,0)$ forbidden reflections. As shown in Fig. 8, the real anisotropy axis remains very close to this direction, and this can be related to the fact that for these reflections the smaller-cluster approximation gives a rather accurate description. Therefore, even though it is obvious that the occurrence of RXS implies an electric quadrupole moment at Mn sites in the ground state, its symmetry (e.g., its principal axes) cannot be inferred from the ASF tensor.

In conclusion, all measured resonant forbidden reflections at the Mn *K* edge in $LaMnO_3$ can be explained within the multiple-scattering theory in terms of long-range order of structural distortions around Mn atoms without invoking any kind of *d*-OO: the temperature dependence of the RXS signal has been found practically flat, thus removing the last obstacle to the full comprehension of its underlying physics. The present results point out that solid-state effects are important and, as for the $(0,0,2n+1)$ reflection, that the ionic localized models do not always work properly to explain in detail the orbital and charge physics of transition-metal oxides.

ACKNOWLEDGMENTS

This work was financially supported by the Spanish CICyT Grant No. MAT2005-04562 project, Diputación General de Aragón (DGA-CAMRADS, PIPO18/2005), and CICyT-INFN agreement. K.H. acknowledges the DGA research grant. The authors thank ESRF for granting beam time.

[1] E. Dagotto, T. Hotta, and A. Moreo, Phys. Rep. **344**, 362 (2001).
[2] Jeroen van den Brink, New J. Phys. **6**, 201 (2004).
[3] A. M. Oles, M. Cuoco, and N. B. Perkins, *Lectures on the Physics of Highly Correlated Electron Systems IV*, edited by F. Mancini, AIP Conf. Proc. No. 527 (AIP, Melville, NY, 2000), pp. 226–380, and references therein.
[4] J. B. Goodenough, Phys. Rev. **100**, 564 (1955).
[5] Y. Murakami, J. P. Hill, D. Gibbs, M. Blume, I. Koyama, M. Tanaka, H. Kawata, T. Arima, Y. Tokura, K. Hirota, and Y. Endoh, Phys. Rev. Lett. **81**, 582 (1998).
[6] S. Ishihara and S. Maekawa, Rep. Prog. Phys. **65**, 561 (2002).
[7] J. García, M. C. Sánchez, J. Blasco, G. Subías, and M. G. Proietti, J. Phys.: Condens. Matter **13**, 3243 (2001).
[8] I. S. Elfimov, V. I. Anisimov, and G. A. Sawatzky, Phys. Rev. Lett. **82**, 4264 (1999); M. Takahashi, J. Igarashi, and P. Fulde, J. Phys. Soc. Jpn. **68**, 2530 (1999).

[9] M. Benfatto, Y. Joly, and C. R. Natoli, Phys. Rev. Lett. **83**, 636 (1999).
[10] Q. Shen, I. S. Elfimov, P. Fanwick, Y. Tokura, T. Kimura, K. Finkelstein, R. Colella, and G. A. Sawatzky, Phys. Rev. Lett. **96**, 246405 (2006).
[11] C. Ritter, M. R. Ibarra, J. M. De Teresa, P. A. Algarabel, C. Marquina, J. Blasco, J. Garcia, S. Oseroff, and S.-W. Cheong, Phys. Rev. B **56**, 8902 (1997).
[12] P. Norby, I. G. K. Andersen, E. K. Andersen, and N. H. Andersen, J. Solid State Chem. **119**, 191 (1995); J. Rodriguez-Carvajal, M. Hennion, F. Moussa, A. H. Moudden, L. Pinsard, and A. Revcolevschi, Phys. Rev. B **57**, R3189 (1998).
[13] M. C. Sánchez, G. Subías, J. García, and J. Blasco, Phys. Rev. Lett. **90**, 045503 (2003).
[14] J. S. Zhou and J. B. Goodenough, Phys. Rev. B **60**, R15002 (1999).
[15] E. O. Wollan and W. C. Koehler, Phys. Rev. **100**, 545 (1955).
[16] J. B. Goodenough, *Magnetism and Chemical Bond* (Interscience, New York, 1963).
[17] F. Moussa, M. Hennion, J. Rodriguez-Carvajal, H. Moudden, L. Pinsard, and A. Revcolevschi, Phys. Rev. B **54**, 15149 (1996); K. Hirota, N. Kaneko, A. Nishizawa, and Y. Endoh, J. Phys. Soc. Jpn. **65**, 3736 (1996).
[18] M. Benfatto, S. Della Longa, and C. R. Natoli, J. Synchrotron Radiat. **10**, 51 (2003).
[19] Y. Joly, Phys. Rev. B **63**, 125120 (2001). The code can be freely downloaded from the web site: http://www-cristallo.grenoble.cnrs.fr/simulation
[20] A. Stunault, C. Vettier, F. de Bergevin, N. Bernhoeft, V. Fernández, S. Langridge, E. Lidström, J. E. Lorenzo-Díaz, D. Wermeille, L. Chabert, and R. Chagnon, J. Synchrotron Radiat. **5**, 1010 (1998).
[21] M. v. Zimmermann, C. S. Nelson, J. P. Hill, D. Gibbs, M. Blume, D. Casa, B. Keimer, Y. Murakami, C.-C. Kao, C. Venkataraman, T. Gog, Y. Tomioka, and Y. Tokura, Phys. Rev. B **64**, 195133 (2001).
[22] M. Blume, J. Appl. Phys. **57**, 3615 (1985); *Resonant Anomalous X-ray Scattering*, edited by G. Materlick, C. Sparks, and K. Fischer (North-Holland, Amsterdam, 1994).
[23] D. H. Templeton and L. K. Templeton, Phys. Rev. B **49**, 14850 (1994).
[24] V. E. Dmitrienko, K. Ishida, A. Kirfel, and E. N. Ovchinnikova, Acta Crystallogr., Sect. A: Found. Crystallogr. **61**, 481 (2005).
[25] S. Di Matteo and C. R. Natoli, J. Synchrotron Radiat. **9**, 9 (2002).
[26] P. Carra, B. T. Thole, M. Altarelli, and X. Wang, Phys. Rev. Lett. **70**, 694 (1993), and references therein.
[27] J. García, G. Subías, M. G. Proietti, H. Renevier, Y. Joly, J. L. Hodeau, J. Blasco, M. C. Sanchez, and J. F. Berar, Phys. Rev. Lett. **85**, 578 (2000); G. Subías, J. García, M. G. Proietti, J. Blasco, H. Renevier, J. L. Hodeau, and M. C. Sánchez, Phys. Rev. B **70**, 155105 (2004).
[28] J. Herrero-Martin, J. García, G. Subías, J. Blasco, and M. Concepcion Sánchez, Phys. Rev. B **70**, 024408 (2004); G. Subías, J. García, P. Beran, M. Nevriva, M. C. Sánchez, and J. L. García-Muñoz, *ibid.* **73**, 205107 (2006).